Jiang Xiangang · Huang Jiahua · Wei Yunwei · Niu Zhipan · Chen Fenghui · Zou Zuyin · Zhu Zhanyuan

The influence of materials on the breaching process of natural dams

Abstract In this study, a series of natural dam overtopping laboratory tests are reported. In these tests, the effect of seven different sediment mixtures on the breaching process was investigated. According to the test results, three stages of the breaching process of natural dams made of different materials were observed. Backward erosion was the primary cause for the incising slopes. The effects of backward erosion became stronger with the larger fines contents of the materials. With an increase in the median diameter (d_{50}) of particles, the breaching time became longer. However, the peak discharge became smaller. With an increase in the fines contents (p), the median diameter of the particles and the void ratio were changed, which resulted in a decrease in the breaching time and an increase in the peak discharge. The breaching time and peak discharge were more sensitive to the median diameter than to the fines contents. The relation between breach width and depth was found to follow a logistic function $W = \frac{\zeta}{1 + e^{(-k(D - D_0))}}$. The parameters ζ, k, and D_0 are defined by a linear relationship with the median diameter and fines content. A breach of the side slope occurred as a tensile failure when the fines contents of the materials were large; otherwise, shear failure occurred. Furthermore, when the materials had fewer fines contents, the volume of the collapsed breach side slope became larger.

Keywords Natural dams · Materials · Breaching process · Breach

Introduction

Natural dams commonly form because of mass movements that block river channels or gullies (Casagli et al. 2003). As a type of natural hazards, natural dams mostly form in mountainous areas where landslides frequently occur. Because the materials of the natural dams have not been compacted and remodeled by humans, the natural dam's internal structure differs from human-made dams (Xu et al. 2009; Li et al. 2011). The large void ratio, soil looseness, poor soil consolidation, and weak soil structure lead to catastrophic bursts (Dong et al. 2011). According to statistics, 41% of natural dams fail less than a week after formation, and 80% within a year (Chai et al. 2001; Ermini and Casagli 2003). There are many cases where natural dams' failures caused damages downstream of the dammed river sections. For example, the Dadu River natural dam broke in 1786, and the severe flood killed 100,000 people (Dai et al. 2005). In 1933, the Diexi natural dam was overtopped 45 days after forming, and a flood of water rushed down the valley for a distance of 250 km, killing at least 2500 people (He et al. 2000). The Yigong River in southeastern Tibet was dammed on April 9, 2000, by a massive landslide with a volume of 300×10^6 m³. The outburst flood damaged many bridges and created numerous new landslides along both banks of the river, which resulted in 30 deaths and caused over 100 people to go missing and over 50,000 to become homeless (Zhu and Li 2001; Shang et al. 2003).

The materials of natural dams are soil-rock mixtures or rocks that came from the slopes of riverbanks. Due to different climate conditions, the degree of rock weathering varies by place, which results in distinctive material differences for different areas. The breaching process may vary significantly because of the differing compositions. Many researchers have attempted to study the influence of materials on the breaching process of dams (Coleman et al. 2002; Morris et al. 2007; Gregoretti et al. 2010; Cao et al. 2011a; Pickert et al. 2011; Schmocker et al. 2014; Chen et al. 2015). The researchers usually analyze the effects of fines contents or median diameters on the discharge or breach size based on three or four types of materials. Although certain qualitative conclusions have been realized, quantitative results are rarely presented due to the few and unrepresentative types of materials used in the tests. For example, the authors have mostly selected fine, medium, and coarse sands as the experimental materials, but the lack of analyses on soil-sand-rock mixtures, which are widespread throughout the world, leave the research incomplete.

The study of the breaching process of natural dams primarily includes the evolution rules of floods, erosion rules, variation rules of breaches, and breach side slopes failure rules. Everything about these four aspects is related to materials. For instance, erosion can directly influence the size of a breach, and its outflow and erosion is affected by the diameter of the materials. Likewise, the strength of the materials depends on variations in the fines and coarse contents and can lead to different slope failure rules. Until now, systematic research on the evolution rules of floods, erosion rules, evolution rules of breaches, and breach side slopes failure rules, which are influenced by materials, has been lacking.

Clay-sand-rock mixtures and sand-rock mixtures have been found to be the most common materials of natural dams based on historical statistics of field screening tests on soils from natural dams (Casagli et al. 2003; Cui et al. 2009; Liu et al. 2010). Therefore, we selected these two material types and configured seven materials by changing their grain compositions to analyze the materials' effects on the breaching process of natural dams. The remainder of this paper is organized as follows. The section "The experimental set-up" describes the experimental set-up. The section "Experimental results" discusses the relationships between material and breaching parameters and proposes a functional relationship that yields the relationships between breaching width and depth. The section "Discussion" also analyzes the influence of materials on slope stability during breaching from the perspective of pore pressure. Finally, the section "Conclusions" reports our conclusions.

The experimental set-up

Experimental materials

The test materials were mixed from clay, sand, and gravel in the laboratory. The colors of the clay, sand, and gravel were distinct
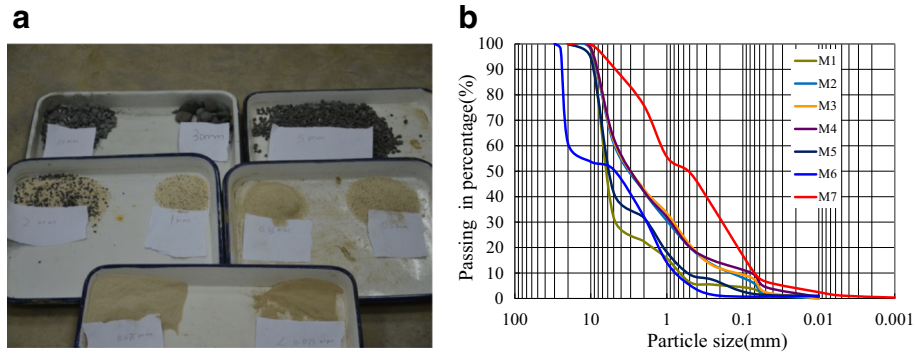
a **b**

Fig. 1 Experimental materials. **a** Photographs of particles. **b** Gradation curves of dam materials

such that the motion of the different particles in the experimental process could be observed. We sieved the clay, sand, and gravel into nine different ranges of particle size: 2–3, 1–2, 0.5–1, 0.2–0.5, 0.1–0.2, 0.05–0.1, 0.025–0.05, 0.0075–0.025, and < 0.0075 cm (Fig. 1a). The seven mixtures used in the tests were designated M1, M2, M3, M4, M5, M6, and M7. The grain size distribution curves of the seven mixed soils are shown in Fig. 1b. The fines contents, p (i.e., particles less than 0.075 mm), of the seven mixtures were 0.38, 3.84, 6.4, 7.9, 1.872, 0.7, and 11.2%, respectively. The median diameters, d_{50}, of the mixtures were 6.2, 3.3, 3.2, 3, 5.8, 5, and 0.52 mm, respectively.

The dams made of the different mixtures had the same dry densities and gravimetric water contents, i.e., 1.72 g/cm³ and 7.82%, respectively. The specific gravity of the fines was tested using the pycnometer method, the coarse particles were tested using the suspending weight method, and the specific gravity of mixtures was determined using the following equation (The Professional Standards Compilation Group of People's Republic of China 1999):

$$G_s = \frac{1}{\frac{p_f}{G_f} + \frac{p_c}{G_c}} \qquad (1)$$

where G_s is the specific gravity of the mixture; p_f and p_c are the fines content and coarse content, respectively (%); and G_f and G_c are the specific gravity of fines and coarse content, respectively. All the specific gravities of the seven materials are listed in Table 1.

Before each test run, we weighed approximately 300 kg materials that fit the gradation curve and watered the composition to satisfy the experimental requirement. The composition was kept in a big plastic bag for 24 h. Then, we mixed the composition with a blender for 1 h to ensure that the materials were homogeneous. The dam was built in three layers, and every layer was compacted until a dry density of 1.72 g/cm³ and height of 10 cm.

Experimental apparatus

The tests were conducted in a flume measuring 15-m long, 0.3-m wide, and 0.6-m deep. The flume was made of glass with a variable bottom slope, and the Manning roughness was approximately 0.01. Figure 2 shows the experimental set-up. The inflow discharge could be accurately controlled with an electromagnetic flowmeter. The dam was located 10 m away from the intake. The tests involved the use of a movable riverbed. The movable riverbed was composed of the same materials as the dam and had a thickness of 5 cm. When the downstream area was a rigid bed, the seepage of the dam bottom that makes contact with the flume was severe. Thus, the seepage flow from the piping easily eroded the dam toe and the dam breach progressively (piping mode). The movable bed could reduce the seepage of dam bottom and prevent piping, which ensured that the dam failure mode was overtopping. At the end of the flume, a 5-cm-high plate was set as the boundary condition. A collection pool was used to collect the sediments and water from the riverbed. A 1-m ruler was pasted to

Table 1 Summary of the experimental test conducted to investigate the influence of the various material parameters on natural dam failures

Test	Channel bed slope (°)	Inflow rate (L/s)	Materials	Maximum diameters (cm)	Median diameters d_{50} (mm)	Fines contents, p (%)	Specific gravity	Void ratio
T-1	7	1	M1	2	6.2	0.38	2.701	0.693
T-2	7	1	M2	2	3.3	3.84	2.702	0.694
T-3	7	1	M3	2	3.2	6.4	2.704	0.695
T-4	7	1	M4	2	3	7.9	2.705	0.696
T-5	7	1	M5	2	5.8	1.872	2.700	0.692
T-6	7	1	M6	3	5	0.7	2.663	0.669
T-7	7	1	M7	2	0.52	11.2	2.704	0.695

The fines in the materials are particles whose diameters were less than 0.075 mm. The specific gravity is the ratio of the density of a substance to that of water, which is a dimensionless parameter
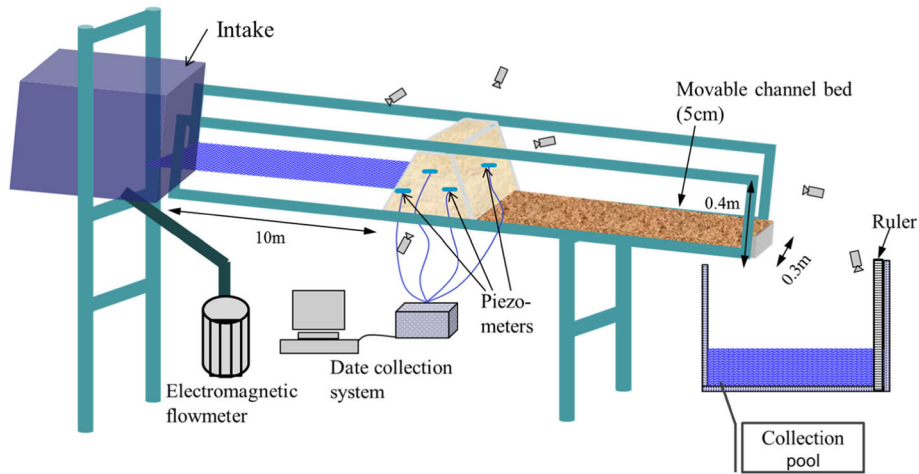
Fig. 2 A sketch of the flume and its hydrological equipment

the wall of the reservoir to measure the height of the fluid contained within. As shown in Fig. 2, six digital video cameras were installed above, on the side of the dam, and above the riverbed and reservoir to record the entire process. Piezometers were installed both upstream of and in the dam as shown in Fig. 2. The piezometers were capable of automatically recording 10 data per second. The piezometers were set in two vertical rows and three horizontal columns. The detailed locations of the piezometers in the dam are shown in Fig. 3. After the first layer of the dam was built from bottom to top and compacted, three piezometers were placed on the layer. The fourth piezometer was placed when the top layer was built and compacted. The sensing wires were fixed to the sidewall of the flume.

Experimental design

A dam with a trapezoidal profile was simulated in the flume tests. The initial upstream and downstream slopes (α, β) of the dams were 20° and 15°, respectively. All of the dams had a common height and width of 0.3 m and a crest width of 0.3 m. A triangular initial breach was set at the side of the dam, of which the depth and top width were 4 cm, and the side slope was fixed at 1:1 (Fig. 4). The inflow discharges used in the experiments were 1 L/s. In total, the experimental designs are summarized in Table 1.

Measurements

The pore water pressure during a breaching process was directly collected by a piezometer that was buried in the dam. The water pressure upstream of the dam could also be tested by the piezometer installed upstream of the dam. Based on the hydrostatic

pressure principle, the water depth could be determined by the water pressure. The error range of measured pore pressure water was 0.0001 kPa. The outflow discharge during the breaching process was calculated from the water depth upstream of the dam. Figure 5 shows a sketch of the natural dam. The angle of the upstream slope of the dam was θ_1, and the angle of the channel was θ_2. After the lake water had overtopped at time t, the water depth in front of the dam was $h(t)$, and the volume of the lake was

$$V(t) = \frac{1}{2}h^2(t)[\cot(\theta_2) + \cot(\theta_1 - \theta_2)]d \tag{2}$$

where d is the width of the flume.

At time $t + \triangle t$, the volume of the lake is:

$$V(t + \varDelta t) = \frac{1}{2}h^2(t + \varDelta t)[\cot(\theta_2) + \cot(\theta_1 - \theta_2)]d \tag{3}$$

Within the time interval $\triangle t$, the outflow discharge is:

$$\frac{V(t) - V(t + \varDelta t)}{\varDelta t} = \frac{1}{2\varDelta t}[h^2(t) - h^2(t + \varDelta t)][\cot(\theta_2) + \cot(\theta_1 - \theta_2)]d \tag{4}$$

In Eq. (4), $h(t)$ is obtained by a piezometer whose accuracy is 0.01 mm. Using the piezometer method, the precision of the discharge is 0.1 L/s.

A camera was installed above the dam, and a ruler that could measure the width of the incised gully was set across the camera. The detailed data on the width of the incised gully were recorded
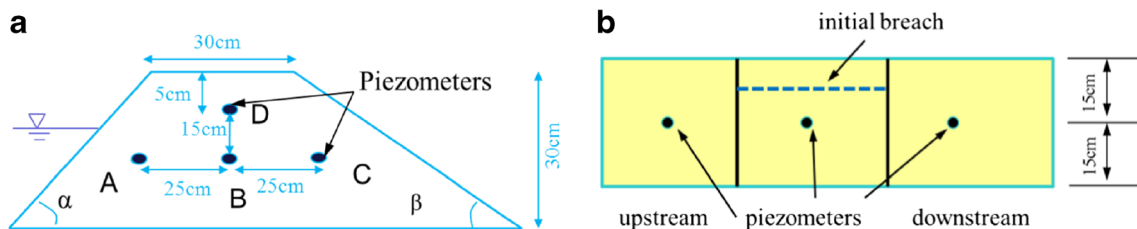
a

b

Fig. 3 The locations of piezometers in the dam. **a** Longitudinal location of the piezometers. **b** Horizontal location of the piezometers
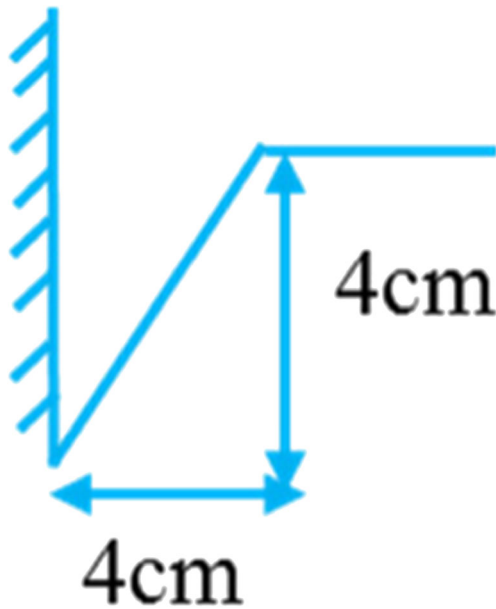
Fig. 4 Dimension of initial breach

on the screen. The height of the bottom of the breach gully was measured with grid paper on the flume glass. The depth of the gully could be determined from this measurement combined with the initial dam height. According to the grid paper, the accuracy of measured breach depth reached to 5 mm. A camera was set behind the grid paper, and the breach depth data were collected during the failure process by video images.

Experimental results

General features

The natural dams made of the seven test materials all failed by overtopping. Figure 6 shows a sequence of images of the dam breaching at different times for the T-5 case. From the experimental results, the dam breaching began with the initial breach, and then the outflow eroded the downstream surface of the dam. Thus, an erosion gully was formed. The gully was continuously eroded and became deeper. During the gully deepening process, its lateral slopes became steeper, and a mass lateral collapse of the gully occurred, which led to the widening of the gully. During this phase of the breaching process, the outflow increased and then decreased with the increase of the breaching time. Moreover, the water-sand mixture flowed muddied and then became clearer with the 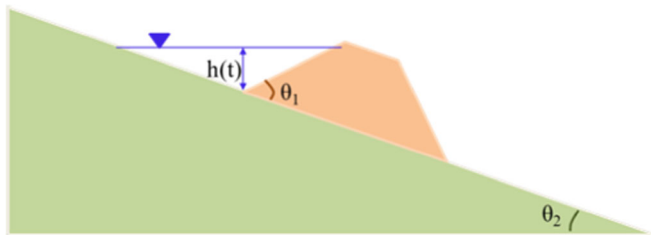development of the breaching. At the end of the tests, the downstream bed channel slopes were larger than the original channels.

The breaching process images illustrated in Fig. 6 were divided into three distinct phases. In the first phase, the breach developed slowly. While the outflow was overtopping the initial channel, its discharge and the velocity was small, and the depth was shallow. Consequently, the erosion ability of the outflow was weak, which slowly decreased the dam height. In this process, the suspended sediment motion was the only form of sediment movement. The breach slope collapsed intermittently, and the volume was small. The breach shape approached that of a rectangle. These observations are consistent with those of Rozov (2003). In the second phase, the breach developed more quickly in the breaching process. With the development of the breach, the outflow eroded more sediment due to larger outflow discharge and the higher flow velocity. The sediments were washed downstream, and the breach developed laterally and vertically simultaneously. In this phase, the shape of the breach channel was similar to an "hourglass," and the shape of the breach was nearly trapezoidal. The breach slope frequently collapsed, and the volume was larger than in the first phase. The third phase was the water and sediment rebalance stage. In this phase, the outflow discharge became small; the flow could erode only fine sand and resulted in the formation of an armoring layer on the surface. This armoring layer protected the sediment that could not be washed away, and the dam height remained constant.

Influence of materials on outflow discharge

During the breaching process, the water depth upstream of the dam was recorded by a piezometer, and the discharge was calculated with Eq. (4). Figure 7 shows the discharge hydrographs for the natural dams composed of the seven materials. This figure shows that the discharge first increased and then decreased. With the dams composed of M5, M6, M1, M2, and M3, the hydrograph present a typical unimodal sort. However, the hydrographs for dams composed of M4 and M7 have multiple peaks. The primary reason for this discrepancy is that the breach of dams composed of M4 and M7 broadened more slowly than the incised dams, and when the failed breach side of the slope could block the breach, the outflow stopped. When the blockage was scattered and pushed away, the water continued to outflow and later reached another peak discharge. Figure 7 also indicates that the hydrographs were shaped into a high, thin type when there were high fines contents in the materials.

Figure 8a reflects the relationship between the peak discharge and median diameter. This figure indicates that the peak discharge decreased with an increase in the median diameter, but the relationship was similar to that between the erosion rate and median diameter (Mitchener and Torfs 1996; Annandale 2006). A significant erosion rate could lead the breach depth to quickly increase, which would increase the water depth in the breach. Based on the broad-crested weir flow equation, a large water depth increases the breach outflow discharge. The results shown in Fig. 8a are consistent with the findings of Coleman et al. (2002). Figure 8b shows how the fines contents affected peak discharge. The figure indicates that, except for with M6, the peak discharge increased as the fines content increased. Although the fines content of M6 was less than M5, the median diameter of M6 was smaller than M5, which is the primary reason that the peak discharge of M6 was larger than M5. Furthermore, these results imply that the peak discharge was more sensitive to the

Fig. 5 Sketch of the natural dam and channel

Fig. 6 Images of the dam at different times for T-5, which shows the gully deepening by overtopping erosion and the characteristic breach phases

median diameter than to the fines content. The fines influenced the discharge by changing the median diameter and void ratio. As the fines content increased and the coarse content decreased, the median diameters decreased (Table 1), which led to a smaller critical shear stress of particles and a larger erosion rate and discharge. The void ratio e can be obtained from

$$e = \frac{G_s(1+w)}{\rho_s} - 1 \qquad (5)$$

where G_s is the specific gravity; w is the gravimetric water content (%); and ρ_s is the density (g/cm³).
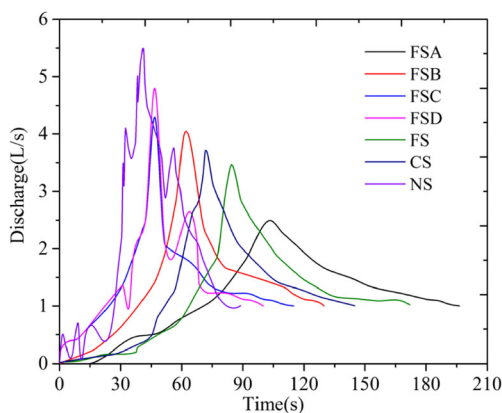

Fig. 7 Breach discharge hydrographs for the seven materials

According to the specific gravities of the seven materials, those of the materials that contained more fines contents (such as M7 and M4) were larger than those of materials with fewer fines content (such as M1 and M6). Large specific gravities led to big void ratios, which increased the erosion rates and discharges.

Influence of materials on incised process

Based on the video images, photographs of the dam shapes at different times were obtained. Then, the profiles of the dam surface were sketched using the photographs. Figure 9 shows the dam surface profiles that were contacting the lateral surface of the flume for the seven materials. During the breaching process, the characteristics of backward erosion existed in the failure process of the dam for the seven materials. The down slopes of breaking grades for M5, M1, and M6, which contained few fines, were gentle. However, the down slopes of the breaking grades for M7, M4, and M3, which contained many fines, were steep and "V"-shaped. This discrepancy indicates that the breaking grades are related to the fines content and may enhance the backward erosion ability of outflow. The interaction forces between the fines particles are the electrostatic attraction, intermolecular forces, chemical-bonding forces, and seepage forces. These interaction forces keep the scarp up the breaking grade stable, and the scarp becomes steeper with the jet impingement action. The erosive sediments resulting from jet impingement are deposited behind the action, and the V shape is formed. The gradient of the down slopes of the breaking grades reflects a backward erosion degree, e.g., a larger gradient of the down slopes of breaking grades denotes that a stronger backward erosion has occurred.

The breach shape is related to many factors, one of which is the water level in the breach. Figure 10 shows the part that was
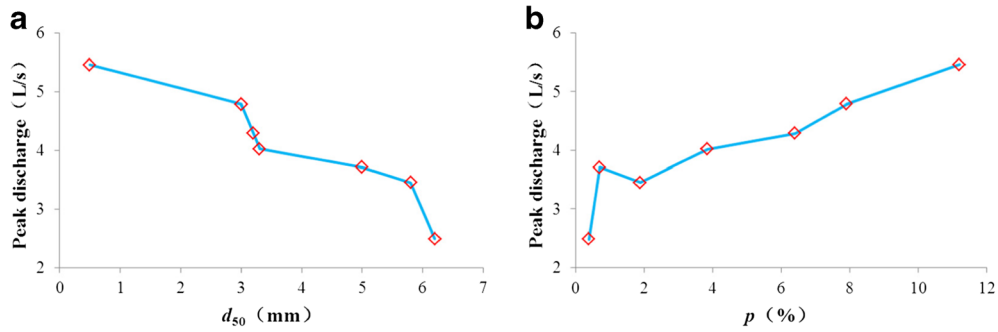
Fig. 8 The influence of the materials on peak discharge. a The relationship between peak discharge and d_{50}. b The relationship between peak discharge and p
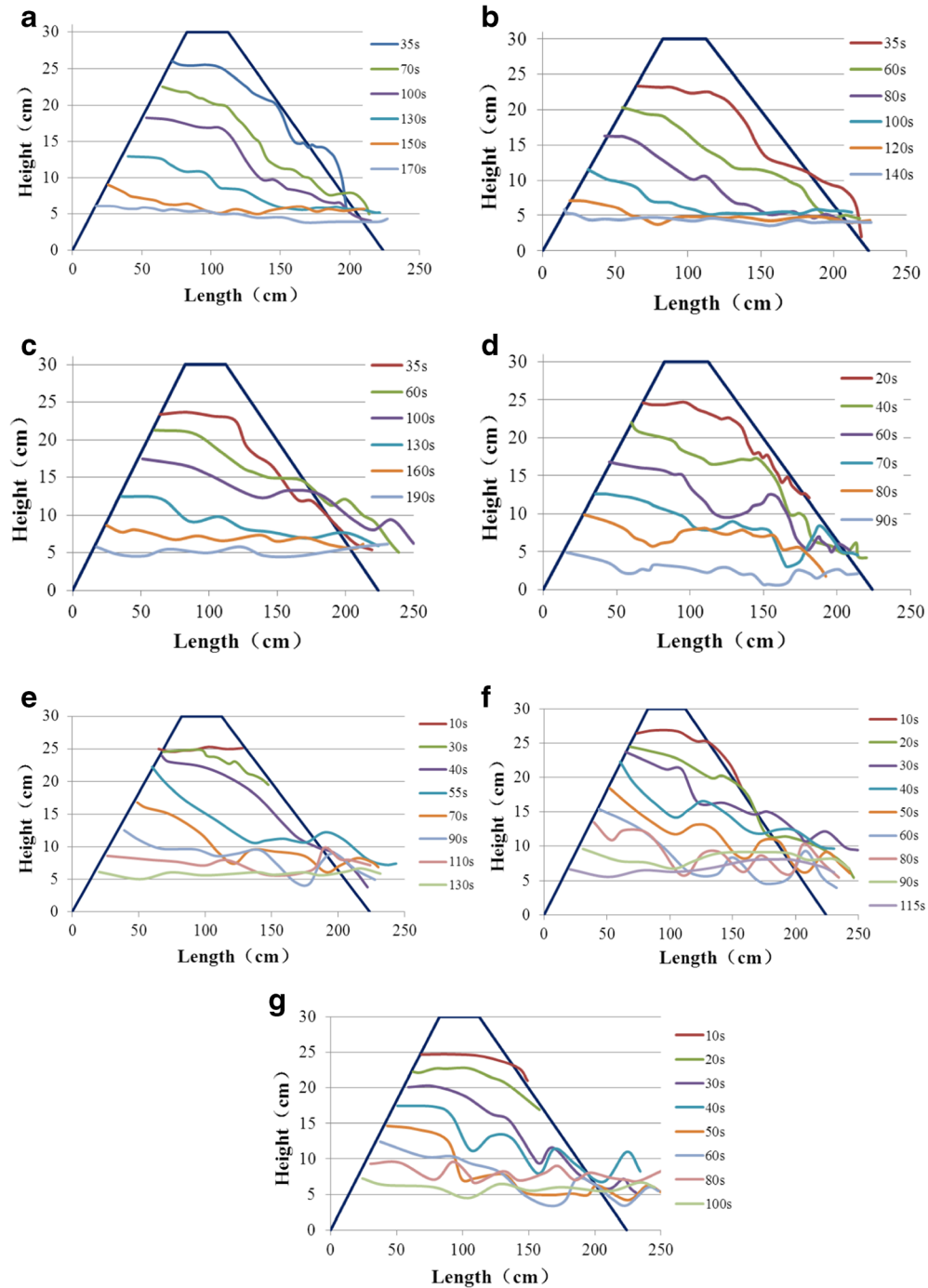

Fig. 9 Development of longitudinal breach bottom profiles for the different materials a M5, b M6, c M1, d M7, e M2, f M3, g M4
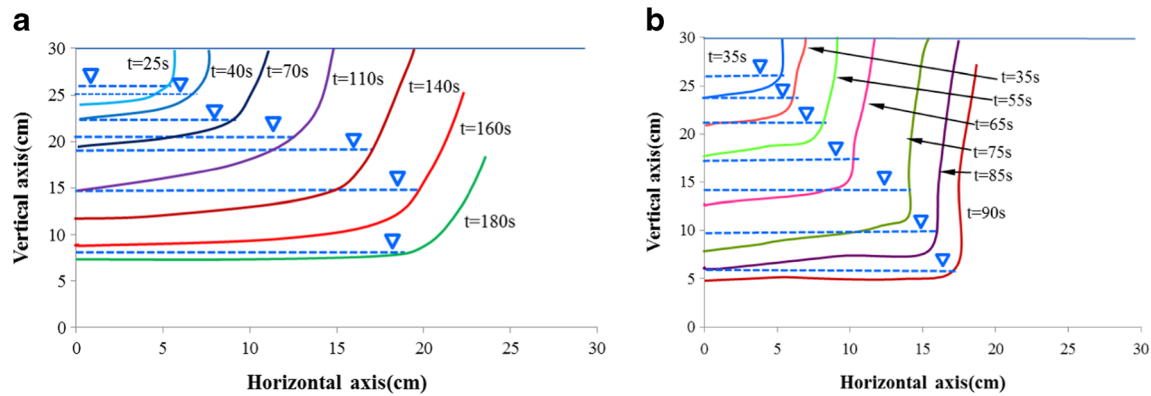
Fig. 10 Development of breach lateral profiles for the different materials. **a** M1. **b** M7

underwater approximated a parabolic shape during the breach development at its initial stages for materials M1 and M7. The part above water approximated a rectangular shape for these two material types. The breach was cutting down with little lateral enlargement as the water level was lower than the breach crest, and the gradient of the breach slopes were almost the same from 70 s to the finish for M1. The later stage shows that the breach width development rate was coincident with the outflow rate. In the next stages, the shape underwater was still nearly parabolic for M1 but caved in the slope for M7. The part above water in these stages was nearly trapezoidal. The breach slope was steeper for M7 than M1 during the failure process. The entire failure process reflects that the per widening rate of M1 was smaller than M7, although the final breach width was bigger for M1 than M7.

Figure 11a indicates that the breaching time of M7, which had the minimum median diameter, was the shortest; the breaching time of M1, which had the maximum median diameter, was the longest. This figure suggests that the breaching time increased with the increasing median diameter. Furthermore, the relationship between the breaching time and median diameter was nonlinear and step-shaped, e.g., with materials having a median diameter in the range 2–3 mm, the breaching time increased more slowly than those with a median diameter in the range 3–4 mm. As shown in Fig. 11b, except for with the M6 material, the breaching time decreased with increasing fines content. Based on Table 1, the median diameter of M6 was smaller than M5, which led to the breaching time of T-6 being less than that of T-5. Moreover, the test materials had larger mean diameters when their fines content was smaller. This relationship suggests that the breaching time was more sensitive to the median

diameter than to the fines content. The primary reason is that the fines in the material have a cementation effect and increase its cohesion. When the fines content is less than 25%, the skeleton is made up of coarse particles, and the fines cannot fill up the porosity between the coarse particles (Vallejo and Mawby 2000). Therefore, the fines cannot bind up particles well for the seven materials in our tests, and the particles initiate by a single granule. In such conditions, the erosion of the material is directly related to the gravity or volume of the particles, i.e., the erosion is related to particles' diameters, which is also true for a cohesionless material. The particles of large diameters are heavier and harder to erode than small particles, which means the erosion rate of larger particles is smaller than that of small particles. Meanwhile, the breaching time is related to the erosion rate (the larger the erosion rate, the shorter the corresponding breaching time). Therefore, the breaching time is more sensitive to the diameter or mean diameter of particles than to the fines content.

Influence of materials on the stability of the breach slope

The materials were composed of fines and coarse particles, and properties of materials were influenced by the fines content or coarse particles content. In this way, we analyzed the stability of the breach side slope as it was affected by the materials' fines contents. With the erosion process development, there was water upstream and in the breach channel, and this water could infiltrate the dam from upstream, breach the channel, and saturate the dam. The pore pressure increased in the saturation area with the erosion process (Fig. 12). Corresponding to the experimental observations, the breach side slope failed when the sharp transient of pore pressure phenomena occurred. Combined with Fig. 9, this outcome indicates that soil
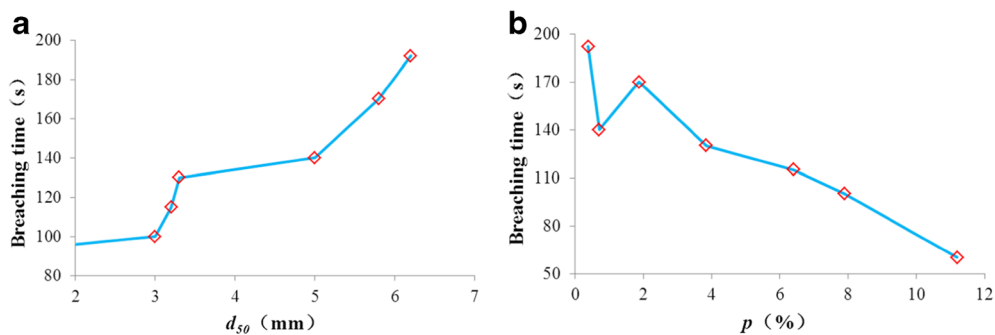

Fig. 11 The relation of (**a**) d_{50} and (**b**) p with the breaching time for all the tests
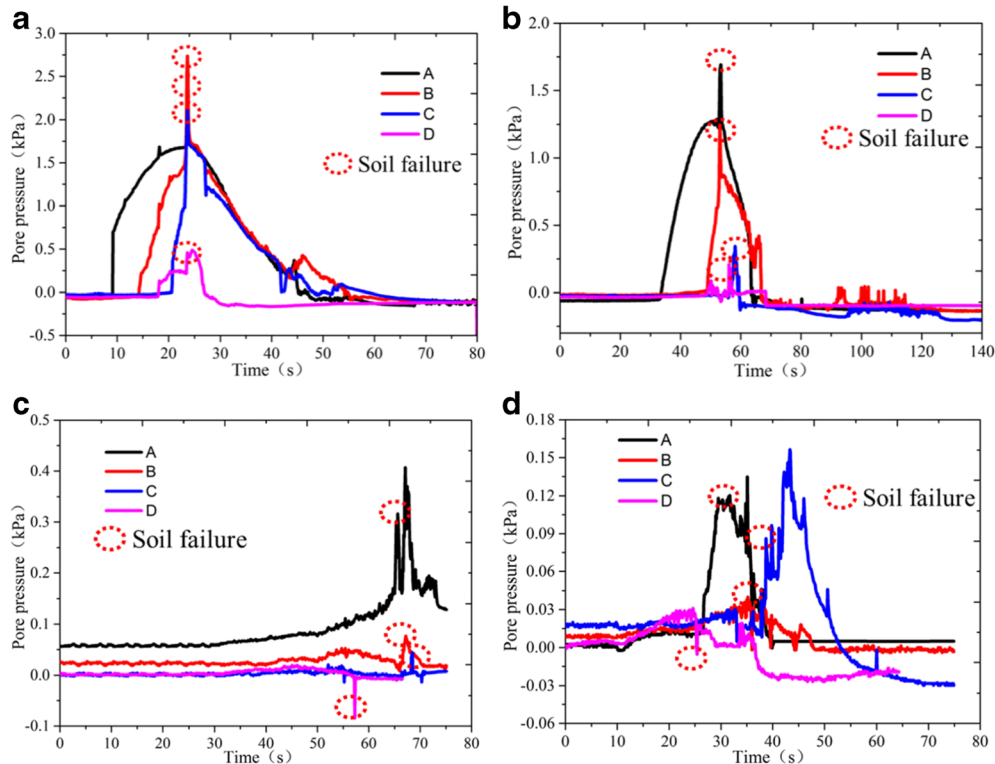
Fig. 12 Time series data of the soil pore pressure at different locations of M7 in the dam. The dam composition was **a** M5, **b** M6, **c** M4, and **d** M7

failure occurs earlier than when the water had eroded to the locations of the piezometers. The evolutions of the pore pressure at different locations for the different materials are distinct. For M5 and M6, which contained fewer fines than M7 and M4, the pore pressures at location D first increased and then decreased at the failure time. However, the opposite was true for M7 and M4, i.e., the pore pressures first decreased and then increased. This reversal indicates that shear failures occurred at location D for M6 and M5. No cracks occurred at the top of the dam, and the failure process was very short. After shear failure, an inclined surface appeared (Fig. 13a, b). The tensile failure occurred at

location D for M7 and M4. Before the tensile failure, a microcrack could be seen at the top of the dam. Moreover, the crack became increasingly wide as time progressed. Then, the breach slope failed at the rotated bottom (Fig. 13c, d). However, shear failure occurred at the other locations (A, B, C) of the four materials. The failure modes were related to the materials. First, the M6 material had few fines so the tensile strength of this material type was very small, and the shear strength was primarily resistant strength. The M4 material had many fines, which led to a larger tensile strength that could resist pulling forces. Second, the M6 material had a larger mean diameter than did M4, which resulted in a lower
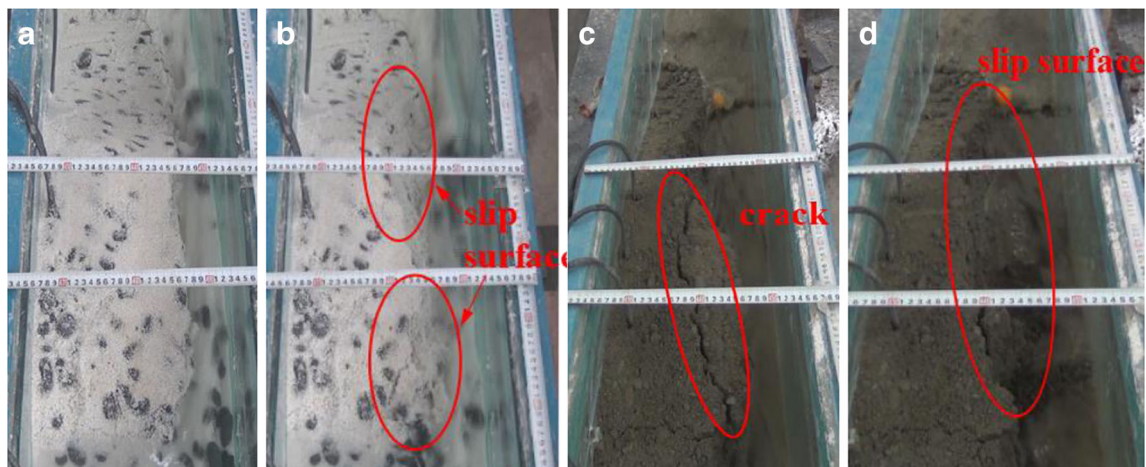

Fig. 13 Images of two failure modes for pre-failure and post-failure. **a** The dam made of M6 materials before shear failure. **b** The characteristics of the dam made of M6 materials after shear failure. **c** The dam made of M7 materials before tensile failure. At this time, a microcrack occurred at the top of the dam. **d** The characteristics of the dam made of M7 materials after tensile failure. The crack became wider and then fell into the breach

erosion rate. In such conditions, the water level decreased more slowly for M6 than M4, and the water could infiltrate the breached slope over more time and a greater saturated area. The infiltrated water could dissolve the soluble salts and quickly reduce the shear strength of the soils. When breach depth reaches a critical height, the shear strength of the slip surface is larger than the resistant shear strength, and then the shear failure occurs (Wu 2013). However, the high erosion rate for the M4 materials led to a rapid decrease in the water level, which resulted in the drainage of the dam with a lowering of the seepage line. This event increased the capillary zone where apparent cohesion and/or tensile strength within the unsaturated soil prevent the material from temporarily collapsing. When the flowing water eroded the breach sides below the water surface and the bottom of the breach, the slope was undermined, and a tension crack progressively developed as the actual tension stress exceeded the soil tension strength, which resulted in tensile failure.

For M6 and M5, the failure times of breach side slope at location A, B, and C were nearly identical. This outcome reflects that the soils at location A, B, and C failed simultaneously, and the volume of the slide should have been large due to the long distance between the three locations. However, for M7 and M4, the failure times of breach side slope at location A, B, and C were different. This outcome reflects that the soils at location A, B, and C failed at different times, and the volume of the slide should have been small, which fits with the observations. In the present experiments, the failure times of breach side slope advanced as the fines contents decreased.

Influence of materials on breach development

Figure 14 shows the relation between the breach width and depth. All the curves in the figure are nonlinear. The curves of M7, M4, and M3, which contained many fines, are almost all below the straight line with a slope of 1. However; the curves of M1 and M6, which contained few fines, are almost entirely above the straight line with a slope of 1. Finally, the curves of M2 and M5 are below the straight line at both ends with the other part of their curves being above the straight line. Overall, the values in the curves decrease as the fines content of the material increased. The overall outcome is that the vertical erosion
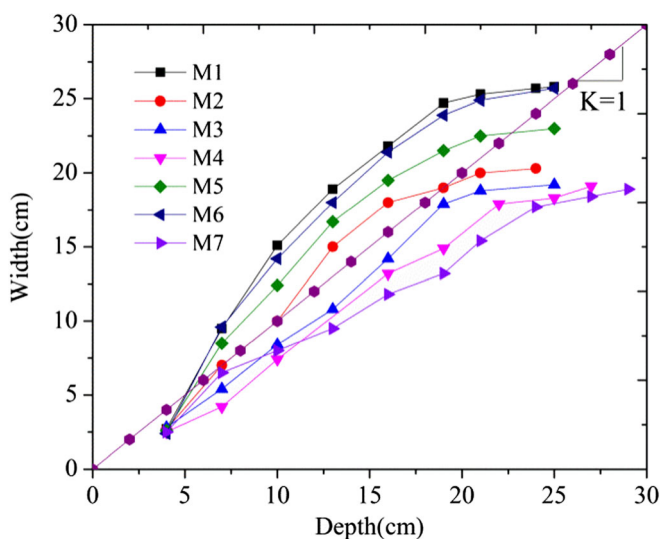

Fig. 14 The relationship between the breach width and depth for different materials

rate increased faster than the lateral erosion rate as the fines were added to the materials; moreover, when the fines were fewer, the breach was wider. The ratio of the final breach width-to-depth gradually tended toward 1 as the fines content decreased.

To obtain the functional relation between the breach width and depth, all the test data were fitted as shown in Fig. 15. This figure shows that all the fitting curves fit the experimental data well, and the fitting curves could be expressed by the following equation:

$$W = \frac{\zeta}{1 + e^{(-k(D-D_0))}} \tag{6}$$

where W is the breach width (cm); D is the breach depth (cm); and ζ(cm), k, and D_0 (cm) are parameters. The variable ζ represents the maximum width that the breach could reach; k stands for the degrees of curvature of the curve. This parameter reflects the breach width growth ratio: when the absolute value of k is large, the breach widens fast; otherwise, the breach widens slowly. The variable D_0 reflects the value of breach depth when the breach reaches half of the final breach width.

To study the influence of material on the breaching parameters, ζ, k, and D_0 were fitted with d_{50} and p. All the data were fitted, which delivered the parameter ζ as the coefficient of d_{50} and p. The same process was conducted for k and D_0, and the results are shown in Fig. 16. The trends of the relationships ζ-d_{50}, k-d_{50}, and D_0-d_{50} are opposite to the relationships ζ-p, k-p, and D_0-p. All the relations follow linear rules, which indicates that ζ, k, and D_0 vary with d_{50} and p monotonically, and the increase of d_{50} (p) can largely increase (decrease) the scale of the breaching width. The parameter ζ appears to increase as d_{50} increases (decreases with increasing p), but the data are somewhat scattered. This outcome reflects that parameter ζ is not sensitive to the median diameter and fines content.

Discussion

An experimental investigation is presented on the influence of materials to the breaching process of a natural dam. In our tests, all the dams failed by overtopping, and this was followed by breaching due to outflowing water. During the breaching process, the outflow water eroded the fines, sands, and gravels, which changed the surface morphology and roughness of the downstream bed and dam breach channel. Therefore, the Manning roughness of the downstream bed and dam breach channel changed constantly. It is obvious that the different Manning roughness values affect the velocity and shear stress of outflow water and influence the backward erosion process of the natural dam. However, it is unclear how the Manning roughness affects the breaching process of the natural dam. This aspect would make interesting research, and we will further study it in the future.

Clearly, the erosion process is associated with the outflow rate and materials. Unlike the development of the breach depth, the breach width develops with both the erosion along the breach channel and the collapse of the side slopes. The particle size, which is a material parameter, directly influences the erosion rate, which has been proven by Van Rijn (1984) and Annandale (2006). It is widely approved that the smaller mean diameters of particles lead
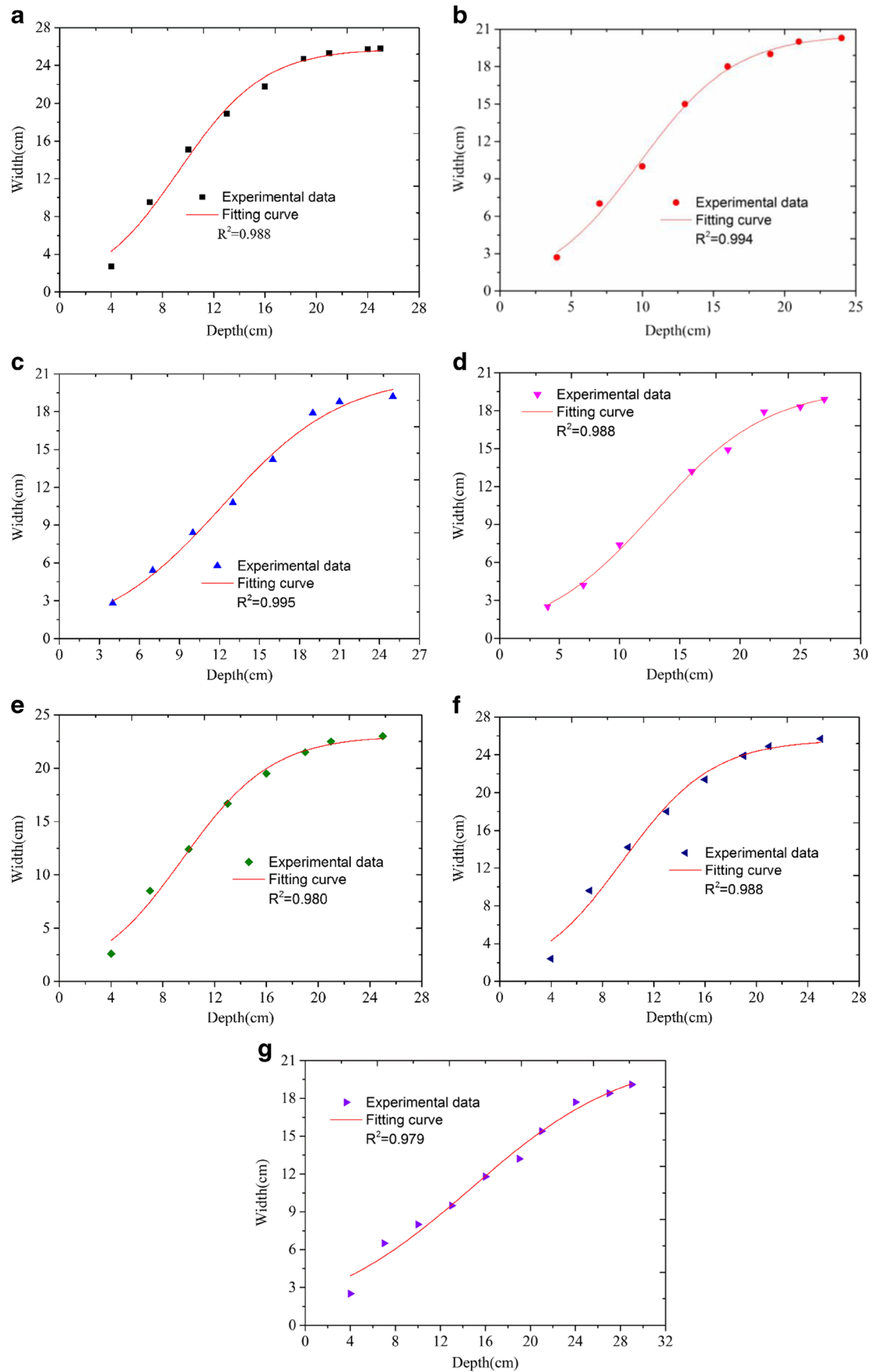
Fig. 15 The comparison to the experimental data with fitting curves. **a** Test T-1. **b** Test T-2. **c** Test T-3. **d** Test T-4. **e** Test T-5. **f** Test T-6. **g** Test T-7
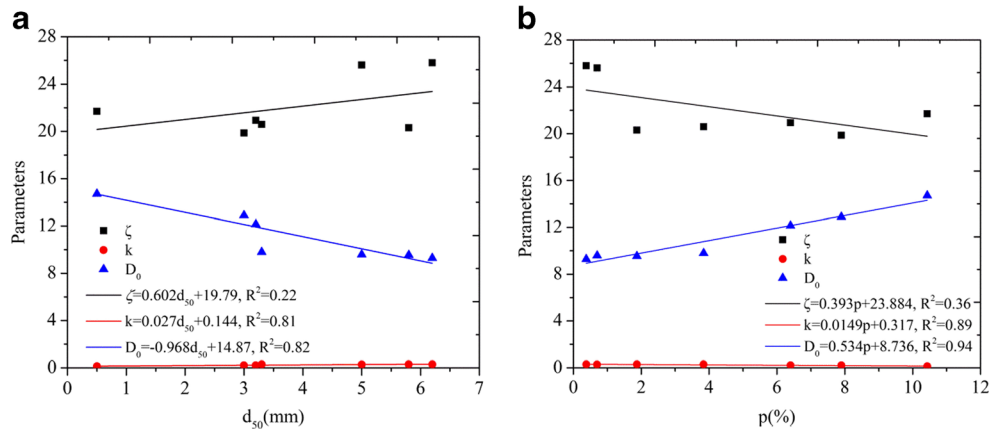
Fig. 16 The influence of d_{50} and p on the parameters ζ, k, and D_0. **a** The influence of d_{50}. **b** The influence of p

to a larger erosion rate. In our tests, the materials with smaller mean diameters had greater erosion rates in the vertical and lateral direction, which led to the breach bottom and a quicker decrease in the water level. Consequently, the time required for the erosion by the outflow of breach slopes of the same height may be shorter for particles with smaller mean diameters than for those with larger diameters. Therefore, the final breach with greater erosion rate may be narrower than that with a lower erosion rate as the erosion time is also considered in the final breach width analysis. The breaching/erosion time is also related to the mean diameter of materials as shown in Fig. 11. Thus, the final breach is related to particle size. On the other hand, the collapse of the side slope was affected by the fines content because the tensile and cohesive strength is generated by fines. Moreover, the tensile and cohesive (shear) strength increases as the fines content increases (Jiang et al. 2016) for a percentage of fines less than 12%, particularly for a small normal stress (the depth of soil is shallow in this paper) (Vallejo 2001). This relation indicates that the breach slope is more stable with more fines in the soils. For a landslide dam with loose deposits, the breach slope collapses more easily for fewer fines,

which results in a quicker breach widening and a larger final breach width. Therefore, the final breach is related to the fines content. The results regarding the final breach width in this paper are identical to those of Pickert et al. (2011).

In this paper, we analyzed the influence of materials on the breaching process, outflow hydrograph and breach geometry. Zhang et al. (2011) analyzed the influence of fine sand and coarse sand on the breaching process of an embankment dam. The results show that the failure processes of dams made of two certain materials have certain same characteristics, such as breaking grade and backward erosion. These characteristics are the same as those found in the results of this study. The relationships between the peak discharge, mean diameter, and fines content in this paper are in good agreement with those found by Coleman et al. (2002) and Zhang et al. (2010). Coleman et al. (2002) and Pickert et al. (2011) studied the breaching process of dams consisting of different materials and recorded the breach width and depth. Figure 17 shows the relationship between the breach width and depth. This figure indicates that the relationships between width and depth also satisfy Eq. (6), as do the results of the tests in this paper. The model proposed by Coleman et al. (2002) was also used to simulate the relationship between breach width and depth during the dam failure. Figure 17 shows some points of measured values deviated from the simulated curves proposed by Coleman et al. (2002). And the simulated values by the model proposed in this paper are closer to measured values than the model of Coleman et al. (2002). Simulation of the overtopping failure of dams in the paper of Coleman et al. (2002) using this model (Eq.(6)) gives reasonable results in comparison to observed and predicted (Coleman et al. 2002). Based on the same experimental conditions, the test results of Coleman et al. (2002) were selected. Due to lack of data regarding fines content of materials, we analyzed the relationships between ζ, k, and D_0 and d_{50}. Figure 18 shows a linear increase in k along when there is an increase in d_{50} and a linear decrease in D_0 as the d_{50} increases, shown in Fig. 16. However, the linear relationship between ζ and d_{50} may not be linear because the data are scattered as experimental data in this paper (Fig. 16).

The above characteristics and the test results agree with those in the paper, but further data may be required to validate the results of this study in the future.
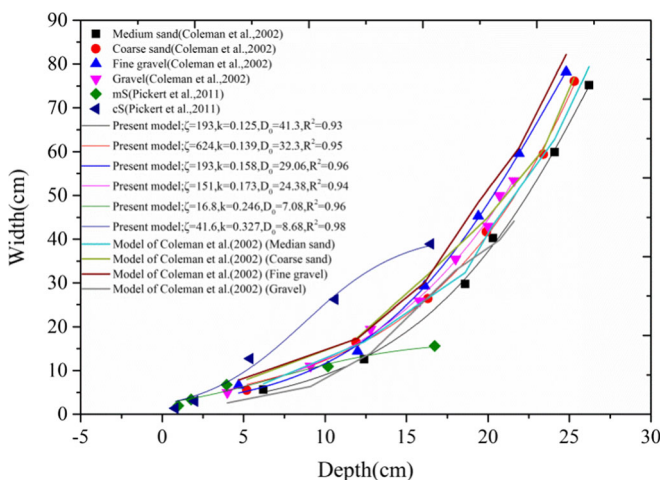

Fig. 17 The relationships between breach width and depth for different materials. The scatter points are measured data by Coleman et al. (2002) and Pickert et al. (2011). Present model is proposed in this paper, i.e., (6). Model of Coleman et al. (2002) is proposed by Coleman et al. (2002)
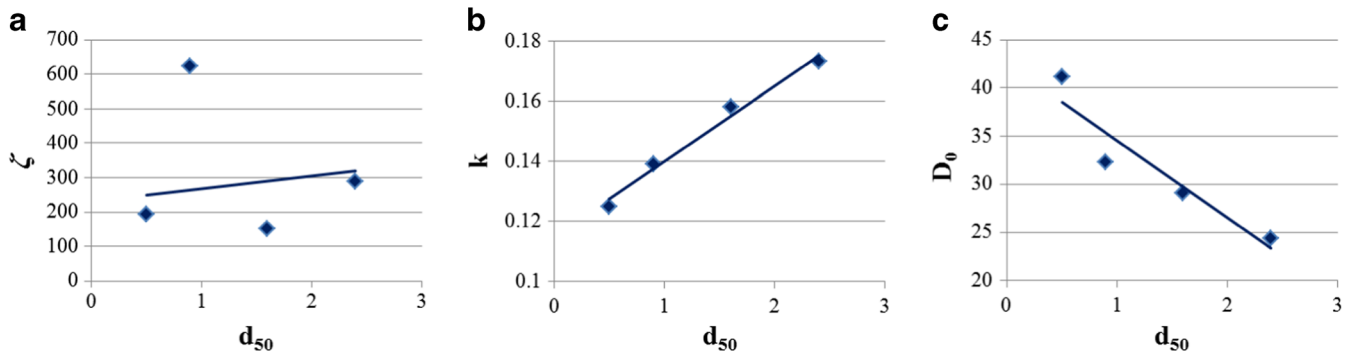
Fig. 18 The influence of d_{50} on the parameters ζ, k, and D_0. The data in this figure are from Coleman et al. (2002) in Fig. 17. **a** The relationship between ζ and d_{50}. **b** The relationship between k and d_{50}. **c** The relationship between D_0 and d_{50}

Conclusions

A series of tests was conducted to investigate the influence of materials on natural dam failure. In the present experiments, overtopping erosion was the primary mechanism of natural dam failure. The breaching process of natural dams composed of different materials was divided into three breach phases. The number of breaking grades increased as the fines content increased, which led to stronger backward erosion.

The peak discharge was increased when the materials had a smaller median diameter and a higher fines content. Moreover, the peak discharges were more sensitive to the median diameter than fines content. Similarly, the breaching time of the natural dam was short when the conditions were a small median diameter and high fines content. The breaching time was more sensitive to the median diameter than to the fines content. The relationship between the breach width and depth was in accord with the function $W = \frac{\zeta}{1 + e^{(-k(D-D_0))}}$. There were linear relationships between the parameters in the function and the median diameter and fines content. Two failure mechanisms of the breach side slope were observed: (a) shear failure and (b) tensile failure. The shear failure mode of the breach side slope was found for natural dams with few fines, and different positions of the breach side slope failed simultaneously. It can be concluded that the volume of the failed breach side slope was larger for a natural dam with fewer fines.

References

Annandale GW (2006) Scour technology: mechanics and engineering practice. McGraw-Hill, New York

Cao Z, Yue Z, Pender G (2011) Landslide dam failure and flood hydraulics. Part I: experimental investigation. Nat Hazards 59(2):1003–1019

Casagli N, Ermini L, Rosati G (2003) Determining grain size distribution of the material composing landslide dams in the Northern Apennines: sampling and processing methods. Eng Geol 69(1):83–97

Chai HJ, Liu HC, Zhang ZY, Liu HW (2001) Preliminarily stability analysis of natural rock-field dam resulting from damming landslide. Geol Sci Technol Inf 20(1):77–81 (in Chinese)

Chen SC, Lin TW, Chen CY (2015) Modeling of natural dam failure modes and downstream riverbed morphological changes with different dam materials in a flume test. Eng Geol 188:148–158

Coleman SE, Andrews DP, Webby MG (2002) Overtopping breaching of noncohesive homogeneous embankments. J Hydraul Eng 128(9):829–838

Cui P, Zhu YY, Han YS, Chen XQ, Zhuang JQ (2009) The 12 May Wenchuan earthquake-induced landslide lakes: distribution and preliminary risk evaluation. Landslides 6(3):209–223

Dai FC, Lee CF, Deng JH, Tham LG (2005) The 1786 earthquake-triggered landslide dam and subsequent dam-break flood on the Dadu river, southwestern China. Geomorphology 65(3):205–221

Dong JJ, Li YS, Kuo CY, Sung RT, Li MH, Lee CT, Lee WR (2011) The formation and breach of a short-lived landslide dam at Hsiaolin village, Taiwan—part I: post-event reconstruction of dam geometry. Eng Geol 123(1):40–59

Ermini L, Casagli N (2003) Prediction of the behaviour of landslide dams using a geomorphological dimensionless index. Earth Surf Process Landf 28(1):31–47

Gregoretti C, Maltauro A, Lanzoni S (2010) Laboratory experiments on the failure of coarse homogeneous sediment natural dams on a sloping bed. J Hydraul Eng 136(11):868–879

He C, Han L, Zhuo Z, Zhi XU (2000) The distribution, causes and effects of damming landslides in China. J Chengdu Univ Technol 27(3):302–307

Jiang XG, Cui P, Chen HY, Guo YY (2016) Formation conditions of outburst debris flow triggered by overtopped natural dam failure. Landslides, 1–11

Li MH, Sung RT, Dong JJ, Lee CT, Chen CC (2011) The formation and breaching of a short-lived landslide dam at Hsiaolin Village, Taiwan—part II: simulation of debris flow with landslide dam breach. Eng Geol 123(1):60–71

Liu N, Chen Z, Zhang JX, Lin W, Chen W, Xu WJ (2010) Draining the Tangjiashan barrier lake. J Hydraul Eng 136(11):914–923

Mitchener H, Torfs H (1996) Erosion of mud/sand mixtures. Coast Eng 29(1–2):1–25

Morris MW, Hassan MAAM, Vaskinn KA (2007) Breach formation: field test and laboratory experiments. J Hydraulic Res 45(sup1):9–17

Pickert G, Weitbrecht V, Bieberstein A (2011) Breaching of overtopped river embankments controlled by apparent cohesion. J Hydraul Res 49(2):143–156

Rozov AL (2003) Modeling of washout of dams. J Hydraul Res 41(6):565–577

Schmocker L, Frank PJ, Hager WH (2014) Overtopping dike-breach: effect of grain size distribution. J Hydraul Res 52(4):559–564

Shang Y, Yang Z, Li L, Liu DA, Liao Q, Wang Y (2003) A super-large landslide in Tibet in 2000: background, occurrence, disaster, and origin. Geomorphology 54(3):225–243

The Professional Standards Compilation Group of People's Republic of China (1999) SL237–1999 Specification of soil test. China Water Power Press, Beijing (in Chinese)

Vallejo LE (2001) Interpretation of the limits in shear strength in binary granular mixtures. Can Geotech J 38(5):1097–1104

Vallejo LE, Mawby R (2000) Porosity influence on the shear strength of granular material–clay mixtures. Eng Geol 58(2):125–136

Van Rijn LC (1984) Sediment pick-up functions. J Hydraul Eng 110(10):1494–1502

Wu W (2013) Simplified physically based model of earthen embankment breaching. J Hydraul Eng 139(8):837–851

Xu Q, Fan XM, Huang RQ, Van Westen C (2009) Landslide dams triggered by the Wenchuan earthquake, Sichuan Province, south west China. Bull Eng Geol Environ 68(3):373–386

Zhang J, Cao SY, Yang FG, Luo LH, Huang E (2010) Experimental study on outlet and scour of blocked dam. J Sichuan Univ (Eng Sci Ed) 5:029

Zhang DW, Huang JC, He XY (2011) Experimental study on overtopping breaching of noncohesive homogeneous embankment dams. Shuikexue Jinzhan/Adv Water Sci 22(2):222–228

Zhu PY, Li T (2001) Flash flooding caused by landslide dam failure ICIMOD Newsletter No 38, available at http://www.icimod.org.np/publications/newsletter/New38/dam.htm

J. Xiangang (✉) · **W. Yunwei** · **C. Fenghui** · **Z. Zuyin** · **Z. Zhanyuan**
College of Civil Engineering,
Sichuan Agricultural University,
DuJiangyan, Chengdu, 611830, China
e-mail: jxgjim@163.com

J. Xiangang · **C. Fenghui**
Sichuan Higher Education Engineering Research Center for Disaster Prevention and Mitigation of Village Construction,
Sichuan Agricultural University,
DuJiangyan, Chengdu, 611830, China

J. Xiangang
Key Laboratory of Mountain Hazards and Surface Process, Institute of Mountain Hazards and Environment,
Chinese Academy of Sciences,
Chengdu, Sichuan 610044, China

H. Jiahua
Department of Civil Engineering,
University of Duisburg-Essen,
Forsthausweg, 47057, Duisburg, Germany

N. Zhipan
State Key Laboratory of Hydraulics and Mountain River Engineering,
Sichuan University,
Chengdu, 610065, China

N. Zhipan
China Three Gorges Projects Development Co., Ltd.,
Chengdu, 610041, China